Regenerative Therapy 26 (2024) 911–921

Contents lists available at ScienceDirect

Regenerative Therapy

journal homepage: http://www.elsevier.com/locate/reth

Original Article

Extracellular vesicle mimetics engineered from mesenchymal stem cells and curcumin promote fibrosis regression in a mouse model of thioacetamide-induced liver fibrosis

Arunnehru Gopal [a, 1], Prakash Gangadaran [a, b, c, 1], Ramya Lakshmi Rajendran [a, c], Ji Min Oh [a, c], Ho Won Lee [a], Chae Moon Hong [a, c, d], Senthilkumar Kalimuthu [a, 2], Man-Hoon Han [e, f], Jaetae Lee [a, d], Byeong-Cheol Ahn [a, b, c, d, *]

[a] Department of Nuclear Medicine, School of Medicine, Kyungpook National University, Daegu 41944, Republic of Korea
[b] BK21 FOUR KNU Convergence Educational Program of Biomedical Sciences for Creative Future Talents, School of Medicine, Kyungpook National University, Daegu 41944, Republic of Korea
[c] Cardiovascular Research Institute, Kyungpook National University, Daegu 41944, Republic of Korea
[d] Department of Nuclear Medicine, Kyungpook National University Hospital, Daegu 41944, Republic of Korea
[e] Department of Pathology, School of Medicine, Kyungpook National University, Daegu 41944, Republic of Korea
[f] Department of Pathology, Kyungpook National University Hospital, Daegu 41944, Republic of Korea

ARTICLE INFO

Article history:
Received 11 July 2024
Received in revised form
30 September 2024
Accepted 10 October 2024

Keywords:
Extracellular vesicles-mimetics
Mesenchymal stem cells
Liver fibrosis
Curcumin

ABSTRACT

Recent research suggests that advanced liver fibrosis could be reversed, but the therapeutic agents needed for the prevention of liver fibrosis remain to be elucidated. The beneficial effects of mesenchymal stem cells (MSCs) and MSC-derived extracellular vesicles (EVs) on liver fibrosis have been reported. However, the large-scale production of MSC-EVs remains challenging. The present study investigated the therapeutic effects of mouse MSC-derived EV mimetics (MEVMs) in combination with curcumin (antifibrotic compound) using a mouse model of thioacetamide-induced liver fibrosis. MEVMs were prepared through the serial extrusion of MSCs. These MEVMs were similar in size and morphology to the EVs. The biodistribution study showed that fluorescently labeled MEVMs predominantly accumulated in the liver. The establishment of liver fibrosis was confirmed via increased collagen (histology), liver fibrosis score, α-smooth muscle actin (α-SMA), and vimentin proteins levels. Treatment with MEVMs, curcumin, or their combination decreased the amount of collagen in liver tissues, with the antifibrotic effects of MEVMs being further confirmed by the liver fibrosis score. All treatments decreased the expression of *collagen 1α*, α-SMA, and vimentin. MEVMs showed superior effects than curcumin. Thus, MSC-derived EVMs could be a potential alternative for the treatment of liver fibrosis.

1. Introduction

The liver is the largest organ in the adult human body, weighing up to 1.5 kg (approximately 2.5 % of the body weight), and consists of hepatocytes and nonparenchymal cells, which include sinusoidal endothelial cells, Kupffer cells, and hepatic stellate cells (HSCs) [1,2]. A recent study reported that liver disease accounts for approximately 2 million deaths per year worldwide, which is around 3.5 % of all deaths worldwide [3]. Liver fibrosis is a tissue repair response to either acute or chronic cellular injury caused by viral hepatitis and alcoholic or non-alcoholic steatohepatitis [4–6]. Advanced chronic fibrosis is described as cirrhosis [7], which is characterized by architectural loss and functional failure leading to life-threatening complications and death. In such cases, liver transplantation remains the only treatment option available; however, a recent study reported that only 10 % of global transplantation needs have been satisfied [3]. Therefore, new strategies for antifibrotic therapies are inevitably warranted.

* Corresponding author. Department of Nuclear Medicine, School of Medicine, Kyungpook National University, Kyungpook National University and Hospital, N101, Gukchaebosang ro 680, Dongin-Dong, Jung-Gu, Daegu, 41944, Republic of Korea.
E-mail address: abc2000@knu.ac.kr (B.-C. Ahn).

Peer review under responsibility of the Japanese Society for Regenerative Medicine.

[1] These authors contributed equally.

[2] Present affiliation: Central Research Laboratory, Swamy Vivekanandha Medical College Hospital and Research Institute, Namakkal 637205, Tamil Nadu, India.

https://doi.org/10.1016/j.reth.2024.10.005

Recent studies have shown that the pharmacological treatment of acute or chronic liver fibrosis can be achieved through the inhibition of hepatocyte death (9,10), activation of HSCs [8,9], inhibition of TGF-β activation [10–12], inhibition of HSC proliferation through receptor tyrosine kinase inhibitors [13–15], and promotion of apoptosis and inactivation of activated HSCs [16–18]. Treatment with inhibitors and antibodies has been found to inhibit liver fibrosis; however, only a few number of preclinical and clinical studies have suggested the reversal of liver fibrosis [19], and liver disease-related mortality has continued to increase [3,20,21]. Over the last few decades, cell-based therapies have emerged as promising approaches for the treatment of various diseases [22,23]. Mesenchymal stem cells (MSCs) can be a promising candidate for cell-based therapies given their multipotency and self-renewing capabilities [24–27]. Recently, numerous reports have suggested that MSC therapies could inhibit liver fibrosis by transforming to hepatocyte-like cells and modulating the liver fibrosis environment through their secretory factors [11,28–30]. The therapeutic potential of cells for liver fibrosis is through the secretome, especially through extracellular vesicles (EVs) [31–34]. Recent evidence has demonstrated that EVs derived from MSCs can be applied as a novel alternative cell-free therapy for liver fibrosis due to their advantages over MSCs [35–38].

EVs are cell-derived nano-sized vesicles that can naturally be released by all types of cells. They are 40–1000 nm in diameter; are capable of carrying biological materials, such as miRNA, mRNA, lipids, proteins, and DNA; and play a vital role in intercellular communication [39,40]. Although recent studies have suggested that EVs are emerging as a cell-free therapeutic strategy, the large-scale production of EVs is necessary to transform from preclinical to clinical, to overcome these issues, recent studies have reported the production of extracellular vesicle mimetics (EVMs), the production of which is 100-fold higher compared to EVs from the same number of cells, to replace the EVs [41,42]. Keunhee oh et al. demonstrated that applying EVMs derived from pancreatic β-cells to bone marrow cells resulted in the efficient differentiation of therapeutic insulin-producing cells [43]. Furthermore, EVMs derived from hepatocytes have the potential for efficient targeted delivery resulting in the promotion of hepatocyte proliferation and liver regeneration, which corroborates finding suggesting that the biological functions of EVMs were similar to natural EVs in several aspects [44].

Curcumin, the polyphenolic substance isolated from rhizome of *Curcuma longa* herb [45], exhibits anti-inflammatory, antioxidant, and antitumor effects [46]. Curcumin has been found to have a therapeutic potential for the prevention of thioacetamide (TAA)-induced liver fibrosis in mice by inducing apoptosis of damaged hepatocytes [47]. Given that EVs from MSCs can prevent liver fibrosis and that EVMs have shown high generation yield with some similar characteristics to EVs, the current study sought to generated EVMs from MSCs (MEVMs) through a simple extrusion method. We investigated whether the generated MEVMs possessed antifibrotic effects for liver fibrosis similar to MSC-EVs [32–34,48]. In addition, we also investigated the effects of combining antifibrotic therapy with curcumin, a well-known antifibrotic agent [45,49,50], along with MEVMs in a mouse model of TAA-induced liver fibrosis.

2. Materials and methods

2.1. Chemicals and antibodies

TAA and curcumin were purchased from Sigma-Aldrich (MO, USA). Primary antibodies such as CD63, ALIX, and GM130 were purchased from Abcam (MA, USA). GAPDH and vimentin were purchased from Santa Cruz (Santa Cruz Biotechnology, TX, USA). α-SMA was obtained from Cell Signaling Technology (MA, USA).

2.2. Cell culture

Mouse bone marrow-derived MSCs were cultured in Dulbecco's modified Eagle's medium/F12 (DMEM-F12, Corning, NY, USA), supplemented with 10 % (v/v) heat-inactivated fetal bovine serum (Merck, NJ, USA) and 1 % penicillin-streptomycin (Gibco, CA, USA). Cells were cultured without contamination and incubated at 37 °C in a humidified atmosphere containing 5 % CO_2. Cells in passage 3–10 were used for this study.

2.3. Preparation of MEVMs

Mouse MSCs were grown up to 80 % cell confluency. Adherent cells were harvested and centrifuged for 3 min (1500 rpm). The cells obtained after centrifugation were counted and resuspended in phosphate-buffered saline (PBS, VWR Chemicals, OH, USA). MEVMs were generated as described in previous studies with slight modification [42,44]. In brief, the cell suspension (2×10^6 cells/mL) was extruded five times through a series of polycarbonate membranes (Nuclepore, Whatman, Inc., NJ, USA) with pore sizes of 10, 5, and 1 μm sequentially using hand-held mini extruder (Avanti polar Lipids, AL, USA). The temperature was maintained at 4°C-8°C for the entire extrusion procedure. Thereafter, the extruded sample was centrifuged at 4000 rpm for 10 min, and the supernatant was passed through a 0.20-μm syringe filter (Corning, NY, USA). The filtered supernatant was transferred to an ultracentrifuge tube (Beckman Coulter, CA, USA) and spun at 100,000×*g* for 1 h at 4 °C using a Beckman Coulter Type SW28 rotor (Beckman Coulter, CA, USA). The obtained MEVM pellet was purified by a differential gradient step using OptiPrep density gradient medium (Iodixonal, Sigma-Aldrich, MO, USA). From the bottom to the top of the ultracentrifuge tube, 1 mL of 60 % iodixanol was added with gentle handling, and 3 mL of 20 % iodixanol was overlaid in the second step. The extruded samples were carefully layered at the top, after which the prepared samples were ultracentrifuged (100,000×*g*, 3 h, 4 °C) using a Beckman Coulter Type SW55ti rotor (Beckman Coulter, CA, USA). The MEVMs were collected manually from the interface of the 60 % and 20 % layers. The total proteins were quantified using a bicinchoninic acid assay (BCA, Thermo Scientific, MA, USA).

2.4. Size measurement via nanoparticle tracking analysis (NTA)

Samples from the MEVMs were diluted to 1:1000 in PBS, after which the size distribution was measured using NTA (NanoSight LM10 instrument, Malvern Instruments, Worcestershire, UK). The supernatant was injected inside the sample chamber without air bubbles using a sterile disposable syringe (Shinchang medical, Gyeongsangbuk-do, Korea) until it extended to the outlet tip of the nozzle. The whole NTA was performed at room temperature. MEVM particles that appear on a black background as a point-scatter movement under Brownian motion were measured. The particle size distribution was analyzed using NTA software (Nanosight, Malvern, Worcestershire, UK) as described previously [51]. Results were presented as the mean size distribution graph and standard deviation (SD) values using the NTA software.

2.5. Transmission electron microscopy (TEM)

Freshly prepared MEVM samples were imaged using TEM as described previously [52]. Briefly, MEVMs isolated by extrusion were resuspended in 2 % paraformaldehyde. Thereafter, the MEVMs

were attached to the Formvar-carbon coated with EM grids (Electron Microscopy Sciences, USA), dried, and then fixed with 1 % glutaraldehyde for 5 min at room temperature. MEVMs in the grids were stained with 2 % uranyl acetate, dried after washing with PBS, and observed under a TEM (HT 7700 Transmission Electron Microscope, Hitachi, Japan) operated at 100 kV.

2.6. Western blotting

The total proteins from MSCs, MEVMs, and fresh liver tissues were extracted to assess protein expression. Briefly, the total proteins from MSCs and MEVMs were suspended in radio immune-precipitation assay (RIPA) buffer. Fresh liver tissue was grounded into a powder using liquid nitrogen, after which all homogenates were suspended with RIPA buffer. Thereafter, total proteins from each sample were vortexed well and immediately kept in ice for 5 min at three times intervals. Afterwards, the sample was centrifuged at 12000×*g* for 20 min at 4 °C, and the concentration was measured from the collected supernatant using a BCA protein assay kit (Thermo Scientific, MA, USA). An equal amount of cells, MEVMs, and liver tissue proteins (20 μg) were separated using sodium dodecyl sulfate-polyacrylamide gel electrophoresis (10 % resolving gel) and then transferred onto a polyvinylidene difluoride membrane (Millipore, MA, USA), blocked with 5 % skim milk (BD, NJ, USA), and then incubated overnight with primary antibodies (CD63, ALIX, GM130, α-SMA, vimentin, and GAPDH) followed by incubation with an HRP-conjugated secondary antibody for 1 h. The dilution used was based on the manufacturer's instructions. The signals were detected after the membrane was incubated in enhanced chemiluminescence (ECL) solution (GE Health Care UK System, Buckinghamshire, UK) using a chemiluminescence analyzer system (Vilber Lourmat, Marne-la-Vallée Cedex, France) [53]. The band intensity was evaluated using GelQuant.NET software (biochemlabsolutions.com).

2.7. Animals

Male C57BL/6 wild-type mice 5–6 weeks of age were obtained from Hamamatsu (Shizuoka-Japan). The animals were housed in a specific pathogen-free environment with free access to standard diet and water. The animal experimental protocol involving mice was approved (KNU-2018-0041) by the Institutional Laboratory Animal Care and Use Committee, Kyungpook National University (KNU, Daegu, Republic of Korea) and were performed in accordance with the guidelines on animal experimentation. Methods of Sacrifice: Cervical Dislocation (Breaking the neck, causing rapid death, suitable for small animals). Methods of Anesthesia: Inhalation anesthesia (2.5 % of isoflurane, Merial, Lyon, France). Efforts to Alleviate Suffering: Humane handling (handled animals gently and minimize stress during procedures).

2.8. Ex vivo imaging of dye-labeled MEVMs

MEVMs were labeled with lipophilic tracer 1,1′-Dioctadecyl-3,3,3′,3′-Tetramethylindodicarbocyanine Perchlorate (DiD, Thermo Fisher Scientific, MA, USA), and fluorescent imaging (FLI) of the labeled MEVMs was performed as described previously [52]. Briefly, MEVMs were incubated with Vybrant DiD cell tracers for 20 min at room temperature. The labeled suspension was washed with PBS and then ultracentrifuged at 100,000×*g* for 1 h. The excess dye was removed and subjected to purification using two-step OptiPrep density gradient ultracentrifugation at 100,000×*g* for 3 h). Thereafter, the final DiD-labeled MEVM ($MEVM^{DID}$) preparation was obtained. $MEVMs^{DID}$ (50 μg) or PBS were then intraperitoneally injected into C57BL/6 mice (n = 3 for each group). At 24 h after the injection, the mice were euthanized, and various tissues were harvested (liver, spleen heart, lungs, and kidney) for *ex vivo* imaging. Then, FLI was performed using an *in vivo* imaging system (IVIS Lumina III Instrument, PerkinElmer, MA, USA) with an excitation of 644 nm and an emission of 665 nm.

2.9. Establishing a mouse model for TAA-induced liver fibrosis

Mice in the positive control group (PC group, n = 23) and normal group (N group, n = 7) were administered TAA and distilled water, respectively, for 4 weeks to generate a mouse model of liver fibrosis. Control (normal) mice (n = 7) received sterile distilled water three times weekly through intraperitoneal injection. Fresh TAA was prepared with sterile distilled water (200 mg/kg of body weight) and administered to PC group mice through intraperitoneal injection for 4 weeks (weekly three times) to induce liver fibrosis. After 3 weeks, normal (n = 2) and TAA-administered (n = 4) mice were sacrificed, and their livers were dissected. Fresh liver tissue was grounded into a powder in a mortar and pestle using liquid nitrogen. The homogenate samples were collected in TRIzol solution (Invitrogen, MA, USA) and RIPA buffer (Thermo Scientific, MA, USA) used for mRNA and protein expression analysis, respectively [54]. In addition, formalin-fixed paraffin-embedded (FFPE) liver sections (4 μm) were used for hematoxylin and eosin (H&E) and Masson's trichrome staining to histologically confirm liver fibrosis in the mouse models. Tissue morphology was evaluated and scored. The amount of collagen (blue stain) in Masson's trichrome, which indicates the positive fibrotic area, was evaluated, and fibrosis stage was determined by a pathologist using the Ishak scoring method on a scale of 0–6 [55].

2.10. Treatment

The normal group (N) served as the control (distilled water). Mice treated with TAA for four consecutive weeks were divided into the following four treatment groups (n = 5 per group): Positive control group (PC; mice treated with PBS twice weekly for 3 weeks); MEVM group (mice treated with 50 μg of MEVMs twice weekly for 3 weeks); Cur group [mice treated with 150 mg/kg of curcumin freshly dissolved in dimethyl sulfoxide (Daejung, Republic of Korea) and injected twice weekly for 3 weeks]; and the combination group (MEVM-Cur; mice treated with both MEVMs and curcumin as described above on alternate days twice weekly for 3 weeks). All mouse groups were treated via intraperitoneal injection and sacrificed 12 h after the last treatment. The detailed *in vivo* experimental schedule is summarized in Fig. 5. Livers from each animal were dissected, washed, and homogenized as described above to perform mRNA and protein expression analysis. Representative liver tissues were fixed with 10 % formaldehyde, dehydrated, and embedded in FFPE blocks for histopathological examination.

2.11. RNA isolation

Total RNA was isolated manually using TRIzol solution according to the manufacturer's recommendations. Briefly, each sample containing the lysed cells in TRIzol solution was treated with chloroform, precipitated in 0.5 mL of isopropyl alcohol (Merck, NJ, USA), and washed with 80 % ethanol (Merck, NJ, USA). The isolated RNA was quantified using an under ultraviolet (UV) spectrophotometer (DeNovix, DE, USA).

2.12. Reverse transcriptase-polymerase chain reaction (RT-PCR)

Isolated RNA (1 μg) was used to generate complementary DNA (cDNA). Reverse transcription was performed using a high-capacity cDNA reverse transcription kit (Applied Biosystems, MA, USA), and cDNA was prepared according to the manufacturer's instructions. The cDNA was amplified via RT-PCR using Col1-α1 and β-actin as primers [56]. The primers were purchased from Bioneer (Republic of Korea), with their sequences being presented in Table 1. Hot Start Ex Taq DNA Polymerase (Takara, Japan), 10 × reaction buffer, primers, and 1 μL of cDNA (combined total volume of 25 μL) were used for RT-PCR. Thermal cycling parameters were standardized according to each primer, and RT-PCR amplification was done using a thermal cycler (Bio-Rad, CA, USA), which amplified the 373- and 508-base pair (bp) product of Col1-α1 and β-actin, respectively. PCR products were then loaded onto 2 % agarose gels, stained with ethidium bromide, and visualized under UV illumination. Band intensity calculations were performed using GelQuant.NET software (biochemlabsolutions.com) and analyzed.

2.13. Histopathological evaluation

Formalin-fixed, paraffin-embedded liver tissues were sectioned and mounted on slides, deparaffinized, hydrated with graded ethanol in descending order, and then stained in slides with H&E and Masson's trichrome according to established protocols. The slides were examined using an Eclipse 80i microscope (Nikon; Tokyo, Japan), and representative images were captured using a Nikon digital sight DS-Fi2 (Nikon, Tokyo, Japan) attached to the microscope. Ishak scorings were measure as mention above.

2.14. Statistical analysis

Statistical analysis was performed using GraphPad Prism5 software version 5.01 (GraphPad Software, Inc., CA, USA). All data were evaluated and expressed as mean ± SD. The level of significance was defined as $P < 0.05$ (*), $P < 0.01$ (**), $P < 0.001$ (***).

3. Results

3.1. Generation of MEVMs

EVMs generated from mouse bone marrow-derived MSCs are shown in Fig. 1. Briefly, MSCs were extruded through membranes (10, 5, 1 μM) one by one (Fig. 1A). After passing the MSCs through a 0.45-μM filter, the supernatant was subjected to ultracentrifugation (Fig. 1B) and OptiPrep density gradient ultracentrifugation (Fig. 1C and D). Purified MEVMs were collected from the interphase between 20 % and 60 % OptiPrep density gradient (arrows indicate MEVMs).

3.2. Characterization of MEVMs

MEVM size was first measured using NTA. Our results showed that MEVMs peaked at a diameter of 103 nm (Fig. 2A), with an average diameter of 151.78 ± 28.6 nm (Fig. 2B). Secondly, the morphology of MEVMs was visualized using a TEM. Our results showed the classical round morphology typical of EVs (Fig. 2C). Finally, we confirmed the presence of EV biomarkers in MEVMs through Western blotting. Our results showed that MEVMs were positive for CD63 (a tetraspanin protein marker) and ALIX (endosomal trafficking protein marker), both of which are well-known EV biomarkers. MEVMs were also positive for GM130 given the membrane contribution from the Golgi apparatus membrane (Fig. 2D). These results suggest that MEVMs were successfully generated from MSCs, with EVs showing typical size, morphology, and biomarkers.

3.3. Biodistribution of $MEVMs^{DID}$ in C57BL/6 mice

After the successful generation and purification of MEVMs, we determined whether intraperitoneally injected MEVMs could target the liver to treat fibrosis therein. After labeling the MEVMs with a lipophilic fluorescent dye (DiD), $MEVMs^{DiD}$ were intraperitoneally injected into mice. Fluorescent signals 24 h after injecting $MEVMs^{DiD}$ showed that MEVMs were localized in the liver, lungs, kidneys. No signals were seen in the spleen and heart. Stronger signals were observed in the liver than in the other organs. No signals were observed in the organs of PBS-injected mice (Fig. 3). This result confirms that MEVMs are capable of targeting the liver in mice.

3.4. Establishment of liver fibrosis in C57BL/6 mice

In an attempt to induce liver fibrosis, 6-week-old male C57BL/6 mice were intraperitoneally injected with TAA for 3 weeks, whereas control mice were intraperitoneally injected with distilled water (Fig. 4A). Mouse models of TAA-induced liver fibrosis were confirmed by histological analysis, PCR, and Western blotting. First, H&E staining following TAA administration revealed liver injury patterns, such as bridging fibrosis and collagen deposition, absent in normal livers (Fig. 4B). Masson's trichrome staining demonstrated that liver tissues with TAA-induced fibrosis had more collagen and fibrogenesis areas (yellow arrow) than did normal liver tissues (Fig. 4C). Second, Ishak liver fibrosis score further confirms the TAA-induced fibrosis (Fig. 4D). Third, the protein expression of α-SMA a marker of activated HSCs [57] and vimentin a fibrosis marker [58] was determined in fibrotic and normal liver tissues. Accordingly, we found that α-SMA was absent in normal liver tissues but present in livers with TAA-induced fibrosis and that fibrotic livers showed greater vimentin expression (1.41-fold) than did normal liver tissues (Fig. 4E). These results clearly demonstrated that TAA administration induced liver fibrosis in mice.

Table 1
Oligonucleotide sequences with annealing temperature and product size used for RT-PCR.

Gene	Primer sequence 5′ to 3′	Annealing Temperature (℃)	DNA bases (bp)
Coll α1	F:CAAGGTCCTTCTGGATCAAGTG R:CCTTTATGCCTCTGTCACCTTG	62	373
β-Actin	F:TCCTTCGTTG CCGGTCCACA R:CGTCTCCGGAGTCCATCACA	60	508

Coll α1: Collagen type alpha 1; β-Actin: Beta-actin; F: Forward primer R: Reverse primer.

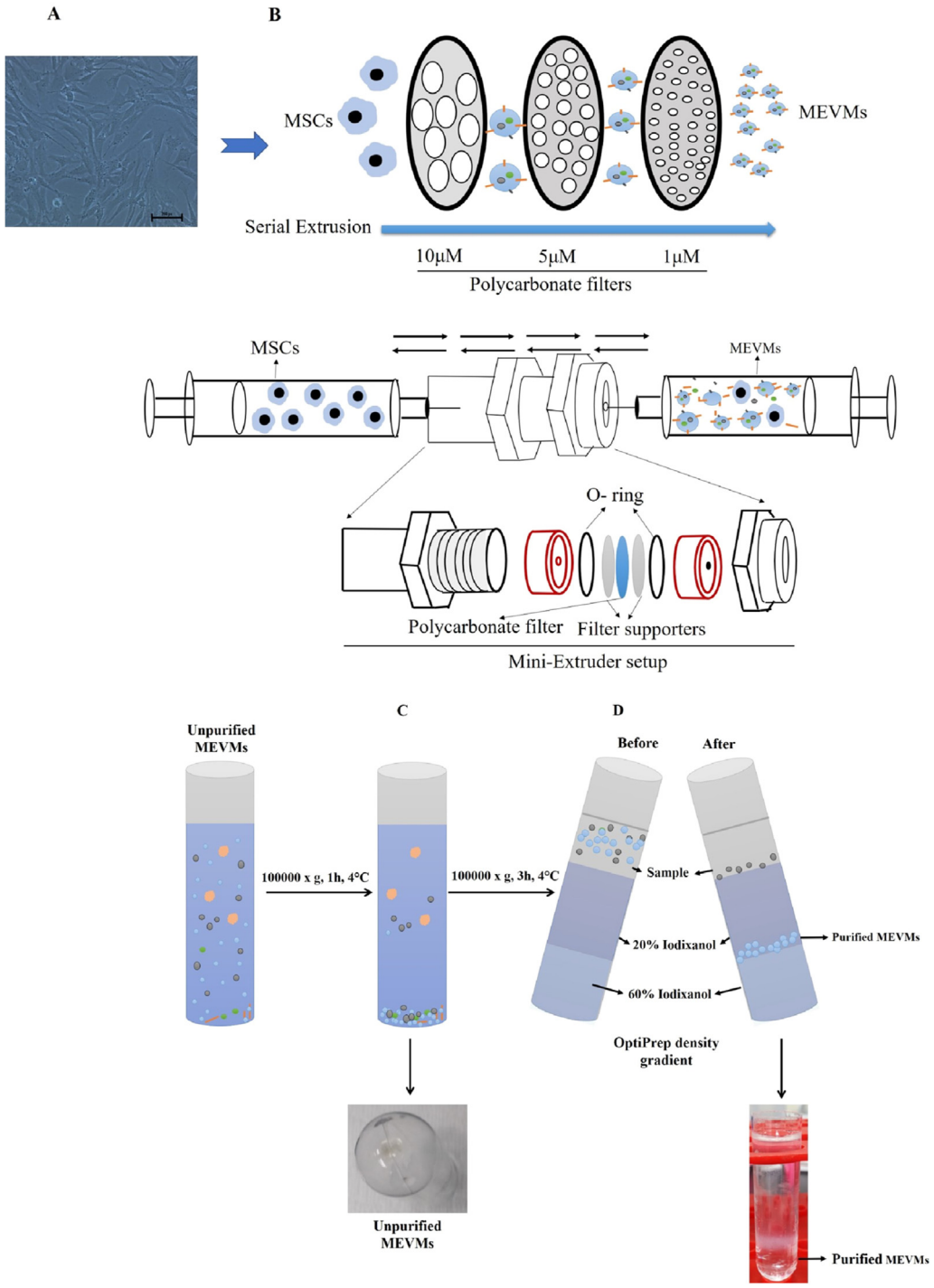

Fig. 1. A Schematic diagram of the preparation of mesenchymal stem cell (MSC)-derived extracellular vesicle (EV) mimetics (MEVMs) through serial extrusion. (A). Mouse MSCs in cells (fifth passage, original magnification: displayed at 20 × , scale bar = 200 px). (B) MSCs were serially extruded through a polycarbonate filter (10, 5, and 1 μm) and ultracentrifuged. (C) MEVM pellets with impurities (fragmented membranes, proteins, and their complexes). (D) MEVMs were purified via two-step OptiPrep density gradient ultracentrifugation (60 and 20 %, respectively), after which purified MEVMs in the interphase between the 60 % and 20 % layers were imaged.

3.5. MEVMs promote fibrosis regression of TAA-induced liver fibrosis in C57BL/6 mice

To determine the *in vivo* effects of MEVMs alone and in combination with the antifibrotic agent curcumin in a mouse model, mice with TAA-induced liver fibrosis were intraperitoneally injected with PBS, MEVMs, or curcumin (Cur) or MEVMs and curcumin (MEVM-Cur). Two injections were administered per week at 3-day intervals for 3 weeks (Fig. 5).

Post-treatment livers were harvested from all groups and subjected to histological [H&E, Masson's trichrome staining, liver fibrosis scoring [55], PCR, and Western blotting analyses. H&E staining showed that livers from the MEVMs or Cur treatment group exhibited lesser liver injury patterns, such as bridging

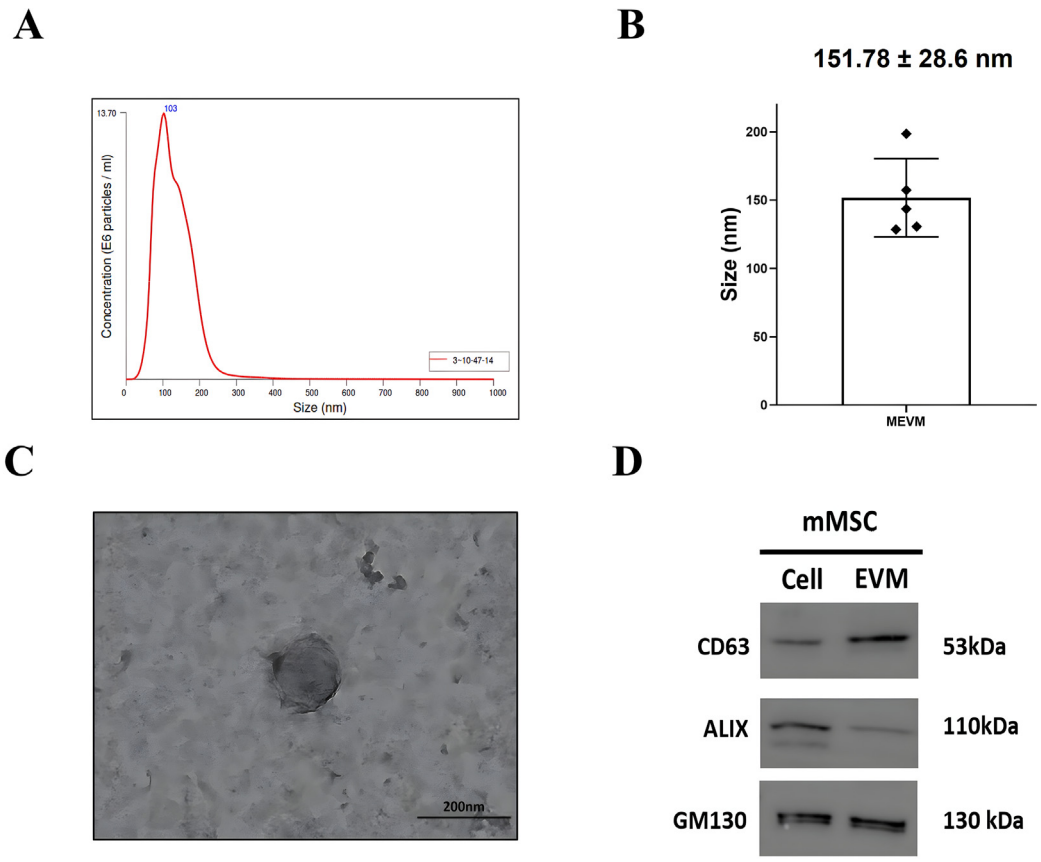

Fig. 2. Characterization of mesenchymal stem cell (MSC)-derived extracellular vesicle (EV) mimetics (MEVMs). (A, B) Distribution of MEVMs by nanoparticle tracking analysis (NTA). Average diameter of MEVMs were analyzed by NTA (n = 5). (C) Transmission electron microscopy of MEVMs (scale bar = 200 nm). (D) Western blotting analysis of MSCs and MEVMs. CD63^{-}, ALIX-, and GM130-specific antibodies were used.

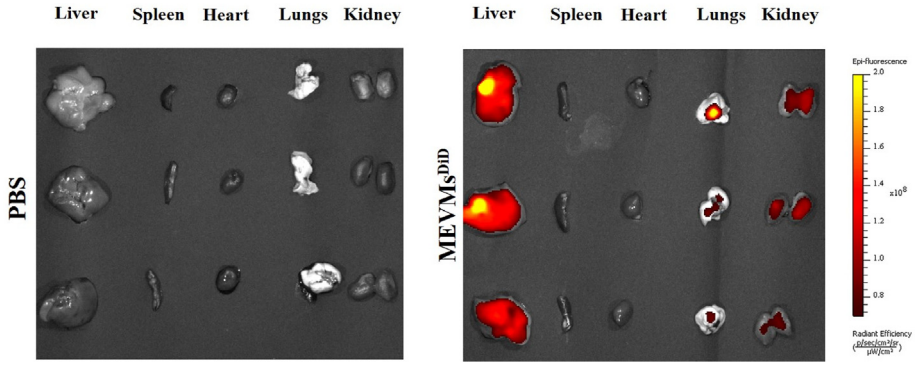

Fig. 3. *Ex vivo* fluorescent imaging of mesenchymal stem cell-derived extracellular vesicle mimetics labeled with a lipophilic fluorescent dye (MEVMs^{DID}) in mice. MEVMs^{DID} or PBS (control) were administered intraperitoneally (n = 3). *Ex vivo* fluorescent signals of MEVMs^{DID} or PBS (control) from major organs in mice were imaged 24 h after injection.

fibrosis and collagen deposition, than did those from the PC group (PBS). Livers from the MEVM-Cur treatment group revealed the least bridging fibrosis and collagen deposition among all treatment groups and looked similar to normal livers (Fig. 6A). In addition, Masson's trichrome staining of liver tissues from the MEVMs or Cur treatment group demonstrated lesser collagen and fibrosis than did livers from the PC group (PBS). Livers from the MEVM-Cur treatment group revealed the least collagen and fibrosis among all treatment groups and looked as similar as normal liver (Fig. 6A). Moreover, Ishak for the Ishak liver fibrosis score further revealed that the MEVM or Cur treatment group had significantly ($p < 0.01$) lower liver fibrosis scores than did the PC group (PBS). The MEVM-Cur treatment group showed a significantly ($p < 0.001$) lower liver fibrosis score than did the PC group (PBS) and a substantially lower score than did the single treatment groups (Fig. 6B).

Moreover, our findings showed that MEVM and Cur treatment group showed a 0.49- and 0.64-fold lower mRNA expression of col1α1, respectively, compared to the PC group (PBS). However, combination treatment (MEVM-Cur) resulted in a 0.34-fold lower col1α1 expression compared to the PC group (PBS) (Fig. 6C).

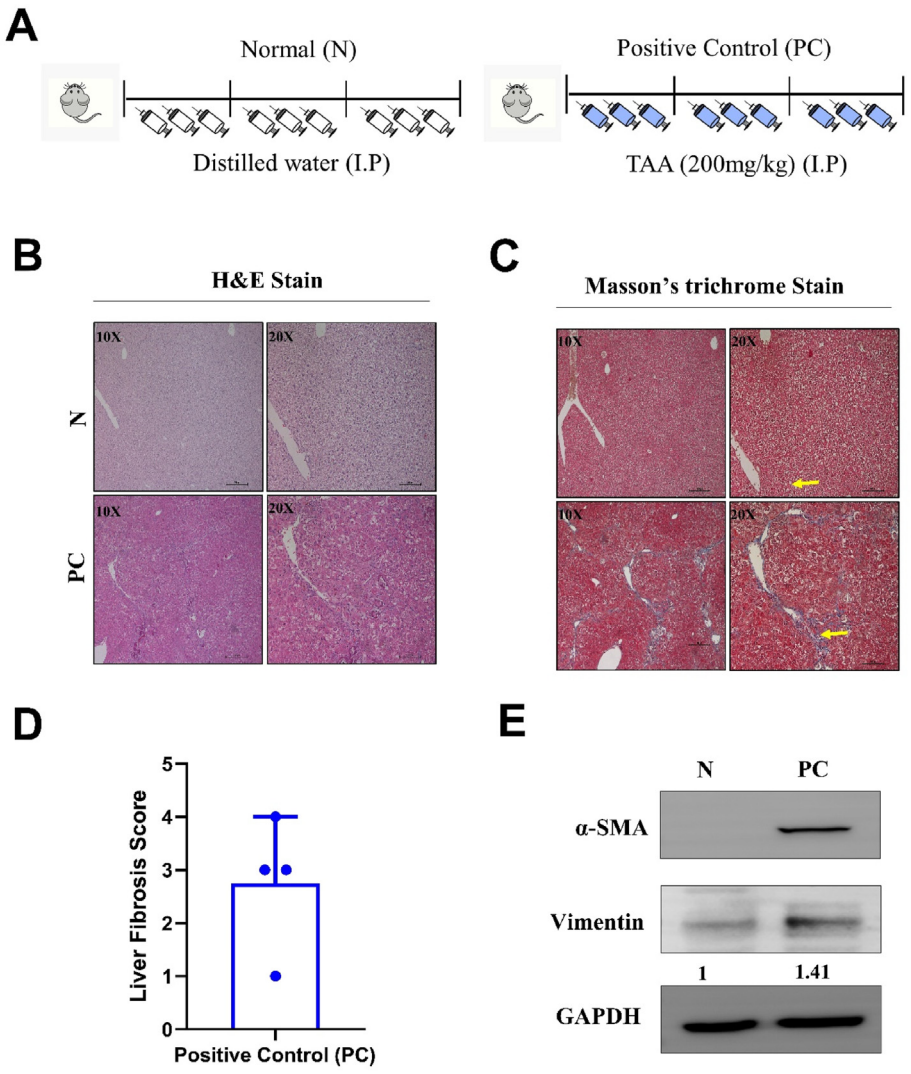

Fig. 4. Establishment of the mouse model of thioacetamide (TAA)-induced liver fibrosis. (A) Schematic overview of the animal experimental setup. Mice were received intraperitoneal injection of TAA (200 mg/kg of body weight). Normal (N) mice (control) were injected with distilled water of equal volume for 3 weeks. Liver tissues were collected from N and PC groups for the evaluation of liver fibrosis. (B, C). Representative images of H&E and Masson's trichrome staining (original magnification: displayed at 10 × and 20 ×, scale bar = 100 μm, respectively). (D) The fibrosis score determined using the Ishak scoring methodology and presented as a bar graph (n = 4). Data were expressed as mean ± SD. (E) Protein levels of α-SMA and vimentin were detected by Western blotting. GAPDH was used as the loading control. Band intensity calculations were performed using GelQuant.NET software. Bridging fibrosis (yellow arrows) was observed in the liver of TAA-treated animals, but no fibrosis was noted in the normal (N) group. Collagen deposition (yellow arrows) was observed in TAA-treated sections but not in the normal (N) group. N group = Normal; PC group = positive control (TAA).

Furthermore, the MEVMs and Cur treatment groups showed a 0.6- and 0.87-fold lower protein expression of α-SMA, respectively, compared to the PC group (PBS). However, combination treatment (MEVM-Cur) induced a 0.46-fold lower α-SMA expression compared to the PC group (PBS) (Fig. 6D). In addition, the MEVMs and Cur treatment groups showed a 0.87- and 0.93-fold lower protein expression of vimentin, respectively, compared to the normal control group. However, combination treatment (MEVM-Cur) promoted a 0.18-fold lower vimentin expression compared to the normal control group (Fig. 6D). These results clearly demonstrated that MEVMs were capable of reducing liver fibrosis and that combined treatment promoted greater reductions in liver fibrosis.

4. Discussion

Liver fibrosis, which results from chronic liver injury, represents a major health problem considering its potential to progress to cirrhosis. The pathology of liver fibrosis is characterized by a multicellular response, including excessive accumulation of ECM proteins. MSC- and MSC-derived EVs are effective for fibrosis regression and liver regeneration. Moreover, MSC-derived EVs have been identified as a promising therapeutic tool for various diseases, including kidney injury, ischemia and regenerative diseases [34,53,59]. Recently, EVMs have emerged as a new strategy for inexpensively producing EV-like EVMs at larger scales in a short amount of time based on previous studies [41,42,52,60]. Nonetheless, the antifibrotic effects of MSC-derived EVMs have yet to be studied. In this study, we hypothesized that MEVMs could promote fibrosis regression of liver fibrosis similar to EVs or exosomes [25,31,32,34]. The present study successfully engineered EVMs from mouse MSCs through simple extrusion and purification. Furthermore, MEVMs were shown to have antifibrotic activity by inhibiting Col1-α1, α-SMA, and vimentin expression in a mouse model of liver fibrosis perhaps due to their cargos. The reduction in liver fibrosis scores further confirmed the antifibrotic activity of MEVMs. Adjuvant therapy with curcumin, a well-known anti-fibrotic agent, further alleviated liver fibrosis along with MEVMs.

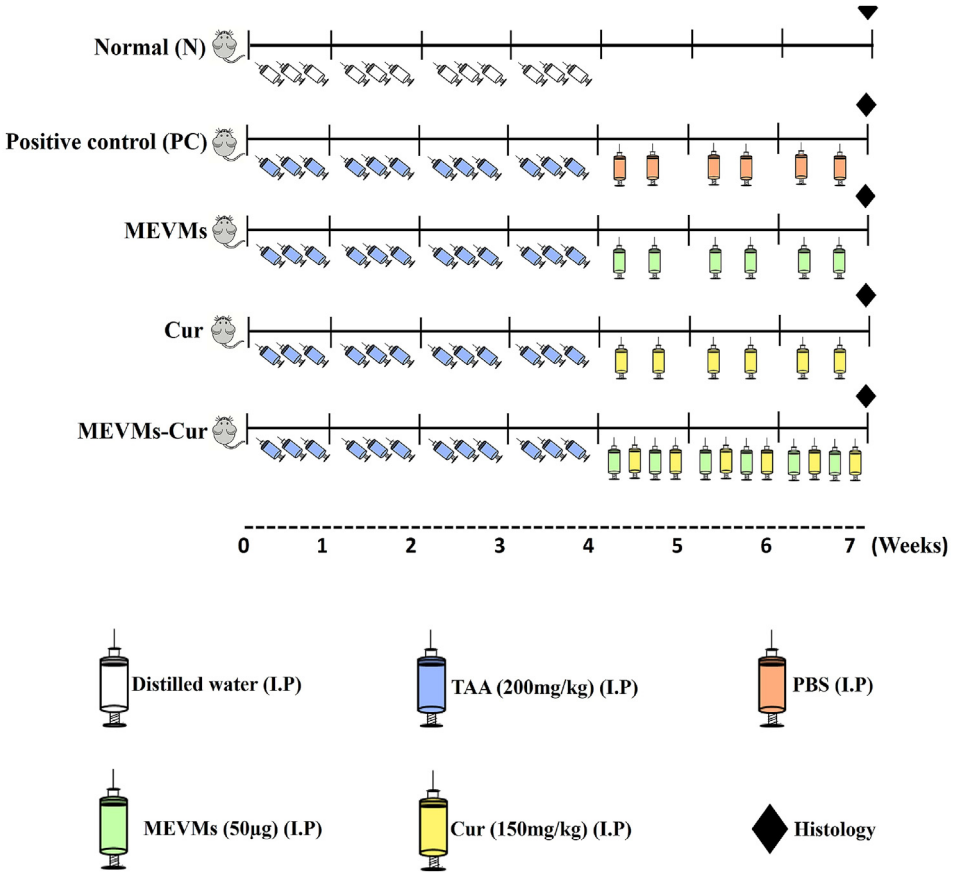

Fig. 5. Schematic illustration of the treatment protocol. Each group of mice except normal (control) received thioacetamide (TAA; 200 mg/kg) through intraperitoneal injection. The normal group was injected with distilled water. Mesenchymal stem cell-derived extracellular vesicle mimetics (MEVMs; 50 µg) or curcumin (150 mg/kg) or MEVMs and curcumin (MEVM-Cur) were administered intraperitoneally twice per week for 3 weeks to each treatment groups (n = 5 per group). The PC group (n = 5) received phosphate-buffered saline (PBS) alone. Mice were sacrificed and their livers excised after 3 weeks of treatment. N group = Normal (no treatment); PC group = positive control, (TAA and PBS); MEVMs = EVMs derived from MSCs, (TAA and MEVMs); Cur group = curcumin, (TAA and curcumin); MEVM-Cur = MEVMs and curcumin (TAA and MEVM-Cur).

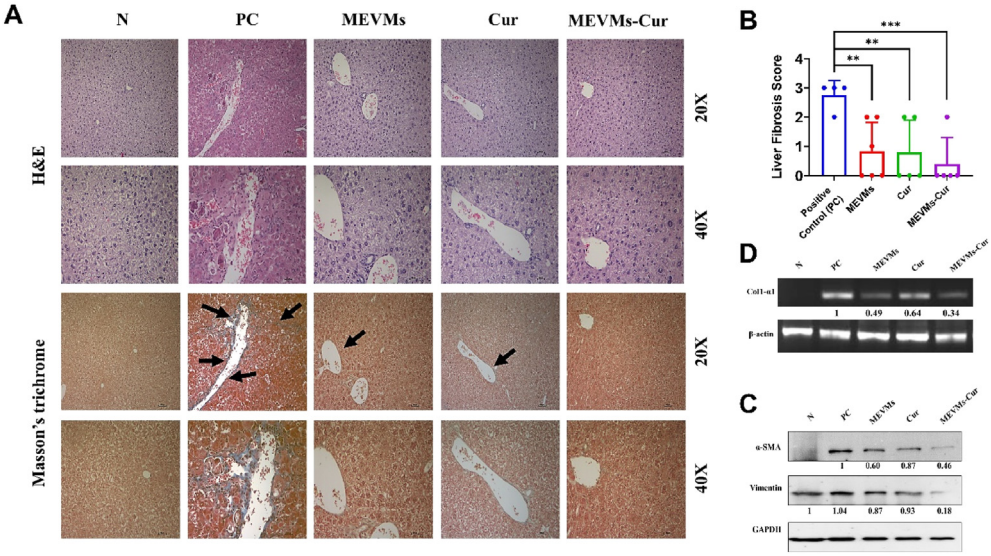

Fig. 6. Effect of mesenchymal stem cell (MSC)-derived extracellular vesicle mimetics (MEVMs) and curcumin on thioacetamide-administered liver tissues. (A) Representative image of histopathological liver sections; H&E and Masson's trichrome staining (magnification: displayed at 20 × and 40 × , scale bar = 100 µm, respectively). (B) The fibrosis score determined using the Ishak scoring methodology and presented as a bar graph (n = 4–6). Data were expressed as mean ± SD, $P < 0.01$ (**), $P < 0.001$ (***); Student's *t*-test was used. (C) mRNA expression of Col1-α1 was performed using reverse transcriptase-polymerase chain reaction. β-Actin was used for normalization. Band intensity was quantified using GelQuant.NET software. (D) Protein levels of α-SMA and vimentin were detected using Western blotting. GAPDH was used as the loading control. Band intensity calculation was performed using GelQuant.NET software. N group = normal; PC group = positive control; MEVMs group = EVMs derived from MSCs group; Cur group = curcumin; MEVM-Cur = MEVMs and Curcumin (combination).

The present results showed that the average diameter of the generated MEVMs was 151.78 nm (range, 30–450 nm). The presence of EV marker proteins CD63 and ALIX were confirmed. Notably, CD63 was more enriched in EVMs than in MSCs. GM130, a Golgi apparatus-related protein, was also present in EVMs, similar to MSCs. These results revealed that MEVMs consists of MSC cell membrane, cytoplasm, and cell organelle proteins. The MEVMs were round in shape, similar to a typical EV. Thus, our findings showed that MEVMs could be successfully generated from MSCs as reported previously [41,42,44].

The main challenge in the attenuation of liver fibrosis is targeting the liver and its fibrotic portions through therapeutic drugs or biological materials [61,62]. The use of DiD, a near infrared fluorescent dye, had a few advantages, including high permeability and constant fluorescence of the extravascular tissue membrane [63]. Therefore, we determined whether or not the intraperitoneal injection of fluorescent dye-labeled MEVMs targeted mouse livers through fluorescence imaging, which is an alternative route of delivery of EVMs to intravenous route. Accordingly, we found greater accumulation of fluorescent dye-labeled MEVMs in the liver than in any other major organs, such as the spleen, heart, lungs and kidneys. While other studies have shown the liver accumulation of EVMs injected through the intravenous route, this has been the first study, to the best of our knowledge, to show the accumulation of MSC-derived EVMs in the liver after being injected through the intraperitoneally route [52,64]. Our imaging of fluorescent dye-labeled MEVMs in mouse was able to determine whether they possess antifibrotic effects in a mouse model of liver fibrosis.

To determine the therapeutic effects of MEVMs in the promotion of liver fibrosis regression, we first need to establish a model of liver fibrosis. A few chemicals, such as carbon tetrachloride, ethanol, and thioacetamide, have been known to induce liver fibrosis and are frequently used to create animal models of liver fibrosis for experimentation [65]. The current study used TAA to induce the liver fibrosis in C57BL/6 mice given that TAA is known to produce adequate fibrosis, has the greatest reproducibility, and shows adequate animal survival for animal experiments [65–67]. We injected TAA through the intraperitoneal route (200 mg/kg per week for a period of 3 weeks) to induce liver fibrosis in mice. We used the intraperitoneal route for TAA administration considering its ability to promote fibrosis faster (i.e., in a few weeks) compared to oral administration (300 mg/L in drinking water), which requires 2–4 months of administration before significant liver fibrosis develops in C57BL/6 mice [68]. Post-TAA administration livers were tested to confirm the development of liver fibrosis in the mice. First, histological analysis and observation confirmed the changes in the morphology of the livers, which included fibrosis, liver cell injury, and collagen accumulation, confirming the results of previous studies [65,68], then liver fibrosis score further confirmed the TAA induced fibrosis [69]. Furthermore, our results showed an increase in the mRNA expression of Col1α1 (a fibrosis marker), protein expression of α-SMA (a marker of activated HSCs), and vimentin (a fibrosis marker), confirming the results of previous studies [33,57,58,70].

After successfully establishing a mouse model of liver fibrosis using TAA, we evaluated the therapeutic effects of MEVMs in promoting liver fibrosis regression with or without the antifibrotic agent curcumin [45,49,50]. Curcumin is a polyphenolic substance with a known therapeutic potency for the prevention in TAA-induced hepatic fibrosis [47]. The current study therefore combined curcumin with MEVMs to determine whether they exhibit additive or synergistic effects in ameliorating liver fibrosis. The current study divided mice into four treatments groups that received PBS, MEVMs, curcumin, and MEVM-Cur twice a week for 3 weeks (see Fig. 5). After 3 weeks of treatments, histological analysis revealed that MEVM treatment reduced collagen accumulation in the liver, with curcumin also showing a comparable reduction in collagen accumulation. However, the MEVM-Cur treatment group showed the lowest collagen accumulation in the liver among all the groups. Our results show, for the first time, that MEVMs alone and combination have antifibrotic effects like naturally secreted EVs from umbilical cord- and amnion-derived MSCs [34,48]. We also showed the antifibrotic effects of MEVMs alone and in combination with curcumin using the well-established Ishak liver fibrosis score, with our results revealing that MEVMs and curcumin alone showed lower liver fibrosis scores than did the control group and that the combination of MEVMs and curcumin promoted the lowest liver fibrosis score. Further molecular analysis showed that MEVMs reduced the mRNA expression of Col1α1 and protein expression of α-SMA and vimentin, suggesting that MEVM treatment was better than curcumin alone. Furthermore, the combination of MEVMs and curcumin showed the most effective in promotion of liver fibrosis regression. Previous studies have shown that exosomes derived from umbilical cord and amnion MSCs reduced the mRNA expression of Col1α1 [34,48] and protein expression of α-SMA [34,48] and vimentin [34], similar to that presented in our study involving EVMs engineered from MSCs. It's important to conduct safety and toxicology evaluations in compliance with regulatory guidelines and standards specific to the intended clinical application of EVMs engineered from MSCs. Such assessments are vital not only for regulatory approval but also to establish the safety and efficacy of EVMs engineered from MSCs-based therapies in clinical practice.

The advantages of the current study are as follows. First, we were able to engineer active and functional EVMs from MSCs through simple methodology. Second, MEVMs can be produced at larger scales compared to EVs or exosomes for future clinical application, Third, MEVMs are capable of targeting the liver *in vivo.* Hence, MEVMs can be loaded with antifibrotic agents to further improve their antifibrotic effects on the liver and protect other tissues and organs for adverse effects of the agents.

5. Conclusions

The results of the current study suggest that MSC-derived EVMs promotes fibrosis regression in the thioacetamide-induced liver fibrosis. This suggests that MEVMs can be used for the treatment of fibrotic liver disease.

Authors contribution

Study conception and design: Gopal A and Ahn B–C; Acquisition of data: Gopal A; Analysis and interpretation of data: Gopal A, Gangadaran P, Rajendran RL, Oh JM, Lee HW and Han M-H; Drafting of manuscript: Gangadaran P and Gopal A; Critical review: Lee HW, Hong CH, Kalimuthu S, Lee J and Ahn B–C; Acquisition of fund and materials: Gangadaran P, Rajendran RL, Ahn B–C; Supervision: Ahn B–C.

Declaration of competing interest

The authors declared no potential conflicts of interest concerning the research, authorship, and/or publication of this article.

Acknowledgment

This research was supported by a grant of the Korea Health Technology R&D Project through the Korea Health Industry Development Institute (KHIDI), funded by the Ministry of Health & Welfare, Republic of Korea (Grant number: HI15C0001) and by a grant of the Korea Health Technology R&D Project, Ministry of

Health & Welfare, Republic of Korea (Grant number: HI16C1501). This research was also supported by Basic Science Research Program through the National Research Foundation of Korea (NRF) funded by the Ministry of Education (NRF-2021R1I1A1A01040732 and NRF-2022R1I1A1A01068652).

References

[1] Freitas-Lopes MA, Mafra K, David BA, Carvalho-Gontijo R, Menezes GB. Differential location and distribution of hepatic immune cells. Cells 2017;6. https://doi.org/10.3390/cells6040048.

[2] Kmieć Z. Cooperation of liver cells in health and disease. Adv Anat Embryol Cell Biol 2001;161:III–XIII. 1–151.

[3] Asrani SK, Devarbhavi H, Eaton J, Kamath PS. Burden of liver diseases in the world. J Hepatol 2019;70:151–71. https://doi.org/10.1016/j.jhep.2018.09.014.

[4] Bataller R, Brenner DA. Liver fibrosis. J Clin Invest 2005;115:209–18. https://doi.org/10.1172/JCI24282.

[5] Schuppan D, Ruehl M, Somasundaram R, Hahn EG. Matrix as a modulator of hepatic fibrogenesis. Semin Liver Dis 2001;21:351–72. https://doi.org/10.1055/s-2001-17556.

[6] Poynard T, Mathurin P, Lai C-L, Guyader D, Poupon R, Tainturier M-H, et al. A comparison of fibrosis progression in chronic liver diseases. J Hepatol 2003;38:257–65. https://doi.org/10.1016/s0168-8278(02)00413-0.

[7] Suk KT, Kim DJ. Staging of liver fibrosis or cirrhosis: the role of hepatic venous pressure gradient measurement. World J Hepatol 2015;7:607–15. https://doi.org/10.4254/wjh.v7.i3.607.

[8] Adorini L, Pruzanski M, Shapiro D. Farnesoid X receptor targeting to treat non-alcoholic steatohepatitis. Drug Discov Today 2012;17:988–97. https://doi.org/10.1016/j.drudis.2012.05.012.

[9] Canbay A, Feldstein A, Baskin-Bey E, Bronk SF, Gores GJ. The caspase inhibitor IDN-6556 attenuates hepatic injury and fibrosis in the bile duct ligated mouse. J Pharmacol Exp Therapeut 2004;308:1191–6. https://doi.org/10.1124/jpet.103.060129.

[10] Fan X, Zhang Q, Li S, Lv Y, Su H, Jiang H, et al. Attenuation of CCl4-induced hepatic fibrosis in mice by vaccinating against TGF-β1. PLoS One 2013;8:e82190. https://doi.org/10.1371/journal.pone.0082190.

[11] Ling H, Roux E, Hempel D, Tao J, Smith M, Lonning S, et al. Transforming growth factor β neutralization ameliorates pre-existing hepatic fibrosis and reduces cholangiocarcinoma in thioacetamide-treated rats. PLoS One 2013;8:e54499. https://doi.org/10.1371/journal.pone.0054499.

[12] de Gouville A-C, Boullay V, Krysa G, Pilot J, Brusq J-M, Loriolle F, et al. Inhibition of TGF-beta signaling by an ALK5 inhibitor protects rats from dimethylnitrosamine-induced liver fibrosis. Br J Pharmacol 2005;145:166–77. https://doi.org/10.1038/sj.bjp.0706172.

[13] Mejias M, Garcia-Pras E, Tiani C, Miquel R, Bosch J, Fernandez M. Beneficial effects of sorafenib on splanchnic, intrahepatic, and portocollateral circulations in portal hypertensive and cirrhotic rats. Hepatol Baltim Md 2009;49:1245–56. https://doi.org/10.1002/hep.22758.

[14] Tugues S, Fernandez-Varo G, Muñoz-Luque J, Ros J, Arroyo V, Rodés J, et al. Antiangiogenic treatment with sunitinib ameliorates inflammatory infiltrate, fibrosis, and portal pressure in cirrhotic rats. Hepatol Baltim Md 2007;46:1919–26. https://doi.org/10.1002/hep.21921.

[15] Paik Y-H, Kim J, Aoyama T, De Minicis S, Bataller R, Brenner DA. Role of NADPH oxidases in liver fibrosis. Antioxidants Redox Signal 2014;20:2854–72. https://doi.org/10.1089/ars.2013.5619.

[16] Parsons CJ, Bradford BU, Pan CQ, Cheung E, Schauer M, Knorr A, et al. Antifibrotic effects of a tissue inhibitor of metalloproteinase-1 antibody on established liver fibrosis in rats. Hepatol Baltim Md 2004;40:1106–15. https://doi.org/10.1002/hep.20425.

[17] Liu X, Xu J, Brenner DA, Kisseleva T. Reversibility of liver fibrosis and inactivation of fibrogenic myofibroblasts. Curr Pathobiol Rep 2013;1:209–14. https://doi.org/10.1007/s40139-013-0018-7.

[18] Koyama Y, Xu J, Liu X, Brenner DA. New developments on the treatment of liver fibrosis. Dig Dis 2016;34:589–96. https://doi.org/10.1159/000445269.

[19] Campana L, Iredale JP. Regression of liver fibrosis. Semin Liver Dis 2017;37:1–10. https://doi.org/10.1055/s-0036-1597816.

[20] Udompap P, Kim D, Kim WR. Current and future burden of chronic nonmalignant liver disease. Clin Gastroenterol Hepatol Off Clin Pract J Am Gastroenterol Assoc 2015;13:2031–41. https://doi.org/10.1016/j.cgh.2015.08.015.

[21] Tapper EB, Parikh ND. Mortality due to cirrhosis and liver cancer in the United States, 1999-2016: an observational study. BMJ 2018;362:k2817. https://doi.org/10.1136/bmj.k2817.

[22] Buzhor E, Leshansky L, Blumenthal J, Barash H, Warshawsky D, Mazor Y, et al. Cell-based therapy approaches: the hope for incurable diseases. Regen Med 2014;9:649–72. https://doi.org/10.2217/rme.14.35.

[23] Heathman TRJ, Nienow AW, McCall MJ, Coopman K, Kara B, Hewitt CJ. The translation of cell-based therapies: clinical landscape and manufacturing challenges. Regen Med 2015;10:49–64. https://doi.org/10.2217/rme.14.73.

[24] Bagno L, Hatzistergos KE, Balkan W, Hare JM. Mesenchymal stem cell-based therapy for cardiovascular disease: progress and challenges. Mol Ther 2018;26:1610–23. https://doi.org/10.1016/j.ymthe.2018.05.009.

[25] Tanna T, Sachan V. Mesenchymal stem cells: potential in the treatment of neurodegenerative diseases. Curr Stem Cell Res Ther 2014;9:513–21.

[26] Cho IK, Hunter CE, Ye S, Pongos AL, Chan AWS. Combination of stem cell and gene therapy ameliorates symptoms in Huntington's disease mice. Npj Regen Med 2019;4:1–9. https://doi.org/10.1038/s41536-019-0066-7.

[27] Musiał-Wysocka A, Kot M, Majka M. The pros and cons of mesenchymal stem cell-based therapies. Cell Transplant 2019;28:801–12. https://doi.org/10.1177/0963689719837897.

[28] Al Ghrbawy NM, Afify RAAM, Dyaa N, El Sayed AA. Differentiation of bone marrow: derived mesenchymal stem cells into hepatocyte-like cells. Indian J Hematol Blood Transfus 2016;32:276–83. https://doi.org/10.1007/s12288-015-0581-7.

[29] Puglisi MA, Tesori V, Lattanzi W, Piscaglia AC, Gasbarrini GB, D'Ugo DM, et al. Therapeutic implications of mesenchymal stem cells in liver injury. J Biomed Biotechnol 2011;2011:860578. https://doi.org/10.1155/2011/860578.

[30] Fang B, Shi M, Liao L, Yang S, Liu Y, Zhao RC. Systemic infusion of FLK1(+) mesenchymal stem cells ameliorate carbon tetrachloride-induced liver fibrosis in mice. Transplantation 2004;78:83–8. https://doi.org/10.1097/01.tp.0000128326.95294.14.

[31] Keshtkar S, Azarpira N, Ghahremani MH. Mesenchymal stem cell-derived extracellular vesicles: novel frontiers in regenerative medicine. Stem Cell Res Ther 2018;9. https://doi.org/10.1186/s13287-018-0791-7.

[32] Tan CY, Lai RC, Wong W, Dan YY, Lim S-K, Ho HK. Mesenchymal stem cell-derived exosomes promote hepatic regeneration in drug-induced liver injury models. Stem Cell Res Ther 2014;5:76. https://doi.org/10.1186/scrt465.

[33] Lou G, Yang Y, Liu F, Ye B, Chen Z, Zheng M, et al. MiR-122 modification enhances the therapeutic efficacy of adipose tissue-derived mesenchymal stem cells against liver fibrosis. J Cell Mol Med 2017;21:2963–73. https://doi.org/10.1111/jcmm.13208.

[34] Li T, Yan Y, Wang B, Qian H, Zhang X, Shen L, et al. Exosomes derived from human umbilical cord mesenchymal stem cells alleviate liver fibrosis. Stem Cell Dev 2013;22:845–54. https://doi.org/10.1089/scd.2012.0395.

[35] Mardpour S, Hassani S-N, Mardpour S, Sayahpour F, Vosough M, Ai J, et al. Extracellular vesicles derived from human embryonic stem cell-MSCs ameliorate cirrhosis in thioacetamide-induced chronic liver injury. J Cell Physiol 2018;233:9330–44. https://doi.org/10.1002/jcp.26413.

[36] Chen X-M, Wang X, Hou Z. Editorial: MSC-derived exosomes in tissue regeneration. Front Cell Dev Biol 2023;11:1293109. https://doi.org/10.3389/fcell.2023.1293109.

[37] Cheng Y, Cao X, Qin L. Mesenchymal stem cell-derived extracellular vesicles: a novel cell-free therapy for sepsis. Front Immunol 2020;11:647. https://doi.org/10.3389/fimmu.2020.00647.

[38] Zheng W, Bian S, Qiu S, Bishop CE, Wan M, Xu N, et al. Placenta mesenchymal stem cell-derived extracellular vesicles alleviate liver fibrosis by inactivating hepatic stellate cells through a miR-378c/SKP2 axis. Inflamm Regen 2023;43:47. https://doi.org/10.1186/s41232-023-00297-z.

[39] Gangadaran P, Hong CM, Ahn B-C. An update on in vivo imaging of extracellular vesicles as drug delivery vehicles. Front Pharmacol 2018;9:169. https://doi.org/10.3389/fphar.2018.00169.

[40] Son SH, Gangadaran P, Ahn B-C. A novel strategy of transferring NIS protein to cells using extracellular vesicles leads to increase in iodine uptake and cytotoxicity. Int J Nanomed 2019;14:1779–87. https://doi.org/10.2147/IJN.S189738.

[41] Kalimuthu S, Gangadaran P, Rajendran RL, Zhu L, Oh JM, Lee HW, et al. A new approach for loading anticancer drugs into mesenchymal stem cell-derived exosome mimetics for cancer therapy. Front Pharmacol 2018;9:1116. https://doi.org/10.3389/fphar.2018.01116.

[42] Jang SC, Kim OY, Yoon CM, Choi D-S, Roh T-Y, Park J, et al. Bioinspired exosome-mimetic nanovesicles for targeted delivery of chemotherapeutics to malignant tumors. ACS Nano 2013;7:7698–710. https://doi.org/10.1021/nn402232g.

[43] Oh K, Kim SR, Kim D-K, Seo MW, Lee C, Lee HM, et al. In vivo differentiation of therapeutic insulin-producing cells from bone marrow cells via extracellular vesicle-mimetic nanovesicles. ACS Nano 2015;9:11718–27. https://doi.org/10.1021/acsnano.5b02997.

[44] Wu J-Y, Ji A-L, Wang Z-X, Qiang G-H, Qu Z, Wu J-H, et al. Exosome-Mimetic Nanovesicles from Hepatocytes promote hepatocyte proliferation in vitro and liver regeneration in vivo. Sci Rep 2018;8:2471. https://doi.org/10.1038/s41598-018-20505-y.

[45] Gutierres VO, Campos ML, Arcaro CA, Assis RP, Baldan-Cimatti HM, Peccinini RG, et al. Curcumin pharmacokinetic and pharmacodynamic evidences in streptozotocin-diabetic rats support the antidiabetic activity to Be via metabolite(s). Evid-Based Complement Altern Med ECAM 2015;2015:678218. https://doi.org/10.1155/2015/678218.

[46] Qiu P, Sun J, Man S, Yang H, Ma L, Yu P, et al. Curcumin attenuates N-Nitrosodiethylamine-Induced liver injury in mice by utilizing the method of metabonomics. J Agric Food Chem 2017;65:2000–7. https://doi.org/10.1021/acs.jafc.6b04797.

[47] Wang M-E, Chen Y-C, Chen I-S, Hsieh S-C, Chen S-S, Chiu C-H. Curcumin protects against thioacetamide-induced hepatic fibrosis by attenuating the inflammatory response and inducing apoptosis of damaged hepatocytes. J Nutr Biochem 2012;23:1352–66. https://doi.org/10.1016/j.jnutbio.2011.08.004.

[48] Ohara M, Ohnishi S, Hosono H, Yamamoto K, Yuyama K, Nakamura H, et al. Extracellular vesicles from amnion-derived mesenchymal stem cells ameliorate hepatic inflammation and fibrosis in rats. Stem Cell Int 2018;2018:3212643. https://doi.org/10.1155/2018/3212643.

[49] Shapiro H, Ashkenazi M, Weizman N, Shahmurov M, Aeed H, Bruck R. Curcumin ameliorates acute thioacetamide-induced hepatotoxicity. J Gastroenterol Hepatol 2006;21:358–66. https://doi.org/10.1111/j.1440-1746.2005.03984.x.
[50] Rivera-Espinoza Y, Muriel P. Pharmacological actions of curcumin in liver diseases or damage. Liver Int Off J Int Assoc Study Liver 2009;29:1457–66. https://doi.org/10.1111/j.1478-3231.2009.02086.x.
[51] Soo CY, Song Y, Zheng Y, Campbell EC, Riches AC, Gunn-Moore F, et al. Nanoparticle tracking analysis monitors microvesicle and exosome secretion from immune cells. Immunology 2012;136:192–7. https://doi.org/10.1111/j.1365-2567.2012.03569.x.
[52] Gangadaran P, Hong CM, Oh JM, Rajendran RL, Kalimuthu S, Son SH, et al. In vivo non-invasive imaging of radio-labeled exosome-mimetics derived from red blood cells in mice. Front Pharmacol 2018;9:817. https://doi.org/10.3389/fphar.2018.00817.
[53] Rajendran RL, Gangadaran P, Bak SS, Oh JM, Kalimuthu S, Lee HW, et al. Extracellular vesicles derived from MSCs activates dermal papilla cell in vitro and promotes hair follicle conversion from telogen to anagen in mice. Sci Rep 2017;7:15560. https://doi.org/10.1038/s41598-017-15505-3.
[54] Méndez V, Avelar E, Morales A, Cervantes M, Araiza A, González D. Methodology A rapid protocol for purification of total RNA for tissues collected from pigs at a slaughterhouse. Genet Mol Res 2011;10:3251–5. https://doi.org/10.4238/2011.December.22.3.
[55] Goodman ZD. Grading and staging systems for inflammation and fibrosis in chronic liver diseases. J Hepatol 2007;47:598–607. https://doi.org/10.1016/j.jhep.2007.07.006.
[56] Zhou J, Zhang M, Atherton SS. Tumor necrosis factor-α–induced apoptosis in murine cytomegalovirus retinitis. Investig Opthalmology Vis Sci 2007;48:1691. https://doi.org/10.1167/iovs.06-1040.
[57] Amer J, Salhab A, Doron S, Morali G, Safadi R. A novel flow cytometry tool for fibrosis scoring through hepatic stellate cell differentiation. Cytometry Part J Int Soc Anal Cytol 2018;93:427–35. https://doi.org/10.1002/cyto.a.23202.
[58] Troeger JS, Mederacke I, Gwak G-Y, Dapito DH, Mu X, Hsu CC, et al. Deactivation of hepatic stellate cells during liver fibrosis resolution in mice. Gastroenterology 2012;143. https://doi.org/10.1053/j.gastro.2012.06.036.
[59] Gangadaran P, Rajendran RL, Lee HW, Kalimuthu S, Hong CM, Jeong SY, et al. Extracellular vesicles from mesenchymal stem cells activates VEGF receptors and accelerates recovery of hindlimb ischemia. J Control Release Off J Control Release Soc 2017;264:112–26. https://doi.org/10.1016/j.jconrel.2017.08.022.
[60] Son SH, Oh JM, Gangadaran P, Ji HD, Lee HW, Rajendran RL, et al. White blood cell labeling with Technetium-99m (99mTc) using red blood cell extracellular vesicles-mimetics. Blood Cells Mol Dis 2020;80:102375. https://doi.org/10.1016/j.bcmd.2019.102375.
[61] Inagaki Y, Kokudo T, Kamiya M, Uno S, Sato M, Kaneko J, et al. A novel liver-specific fluorescent anti-cancer drug delivery system using indocyanine green. Sci Rep 2019;9:1–6. https://doi.org/10.1038/s41598-019-39269-0.
[62] Chen Z, Jain A, Liu H, Zhao Z, Cheng K. Targeted drug delivery to hepatic stellate cells for the treatment of liver fibrosis. J Pharmacol Exp Therapeut 2019;370:695–702. https://doi.org/10.1124/jpet.118.256156.
[63] Grange C, Tapparo M, Bruno S, Chatterjee D, Quesenberry PJ, Tetta C, et al. Biodistribution of mesenchymal stem cell-derived extracellular vesicles in a model of acute kidney injury monitored by optical imaging. Int J Mol Med 2014;33:1055–63. https://doi.org/10.3892/ijmm.2014.1663.
[64] Hwang DW, Choi H, Jang SC, Yoo MY, Park JY, Choi NE, et al. Noninvasive imaging of radiolabeled exosome-mimetic nanovesicle using 99mTc-HMPAO. Sci Rep 2015;5. https://doi.org/10.1038/srep15636.
[65] Yanguas SC, Cogliati B, Willebrords J, Maes M, Colle I, van den Bossche B, et al. Experimental models of liver fibrosis. Arch Toxicol 2016;90:1025–48. https://doi.org/10.1007/s00204-015-1543-4.
[66] Shin G-M, Koppula S, Chae Y-J, Kim H-S, Lee J-D, Kim M-K, et al. Anti-hepatofibrosis effect of Allium senescens in activated hepatic stellate cells and thioacetamide-induced fibrosis rat model. Pharm Biol 2018;56:632–42. https://doi.org/10.1080/13880209.2018.1529801.
[67] Jang JH, Kang KJ, Kim YH, Kang YN, Lee IS. Reevaluation of experimental model of hepatic fibrosis induced by hepatotoxic drugs: an easy, applicable, and reproducible model. Transplant Proc 2008;40:2700–3. https://doi.org/10.1016/j.transproceed.2008.07.040.
[68] Wallace MC, Hamesch K, Lunova M, Kim Y, Weiskirchen R, Strnad P, et al. Standard operating procedures in experimental liver research: thioacetamide model in mice and rats. Lab Anim 2015;49:21–9. https://doi.org/10.1177/0023677215573040.
[69] Goodman ZD. Grading and staging systems for inflammation and fibrosis in chronic liver diseases. J Hepatol 2007;47:598–607. https://doi.org/10.1016/j.jhep.2007.07.006.
[70] Shin G-M, Koppula S, Chae Y-J, Kim H-S, Lee J-D, Kim M-K, et al. Anti-hepatofibrosis effect of Allium senescens in activated hepatic stellate cells and thioacetamide-induced fibrosis rat model. Pharm Biol 2018;56:632–42. https://doi.org/10.1080/13880209.2018.1529801.